Selective and Continuous Oil Removal from Oil-Water Mixtures Using a Superhydrophobic and Superoleophilic Stainless Steel Mesh Tube

Rasouli Seyyedabbas, Rezaei Nima, Zendehboudi Sohrab, Duan Xili, Legge Raymond, Chatzis Ioannis

DOI: 10.1021/acs.langmuir.2c03480

Selective and Continuous Oil Removal from Oil-Water Mixtures Using a Superhydrophobic and Superoleophilic Stainless Steel Mesh Tube

Seyedabbas Rasouli[1], Nima Rezaei[1,2], Sohrab Zendehboudi[1], Xili Duan[1], Raymond Legge[3], Ioannis Chatzis[3]

[1]Faculty of Engineering and Applied Science, Memorial University of Newfoundland, St. John's, NL, Canada
[2]Department of Separation Science, School of Engineering Science, Lappeenranta-Lahti University of Technology, Lappeenranta, Finland
[3]Department of Chemical Engineering, University of Waterloo, Waterloo, ON, Canada

ABSTRACT

Development of continuous oil-water separation processes has applications in treatment of industrial oily wastewater and effective management of oil spills. In this research, the performance of a superhydrophobic-superoleophilic (SHSO) membrane in oil-water separation is investigated through dynamic tests. We investigate the effects of total flow rate and oil concentration on the separation efficiency using an as-fabricated SHSO mesh tube. To construct the SHSO membrane, a tubular stainless-steel mesh is dip-coated into a solution, containing a long-chain alkyl silane (Dynasylan® F8261) and functionalized silica nanoparticles (AEROSIL® R812). The as-prepared SHSO mesh tube illustrates a water contact angle of 164° and an oil contact angle of zero for hexane. The maximum oil separation efficiency (SE) of 97% is obtained when the inlet oil-water mixture has the lowest flow rate (5 cm^3/min) with an oil concentration of 10 vol%, while the minimum oil SE (86%) is achieved for the scenario with the highest total flow rate (e.g., 15 cm^3/min) and the highest oil concentration (e.g., 50 vol%). The water SE of about 100% in the tests indicates that the water separation is not affected by the total flow rate and oil concentration, due to the superhydrophobic state of the fabricated mesh. The clear color of water and oil output streams also reveals the high SE of both phases in dynamic tests. The outlet oil flux is increased from 314–790 (L/m^2·h) by increasing the oil permeate flow rate from 0.5–7.5 (cm^3/min). The linear behavior of cumulative amounts of collected oil and water with time demonstrates the high separation performance of a single SHSO mesh, implying no pore-blocking during dynamic

tests. The significant oil SE (97%) of the fabricated SHSO membranes with robust chemical stability shows the promising potential for industrial-scale oil-water separation applications.

Keywords: Superhydrophobic-Superoleophilic Membrane; Oil Separation; Tubular Mesh System; Operating Conditions; Dynamic Tests

1 INTRODUCTION

Ongoing expansion of industries triggers increased production of oily wastewater, that if it is not treated, imposes negative impacts related to the oil-in-water contaminants on human health and aquatic ecosystems [1]. A typical mining operation generates 140,000 L of oily wastewater every day. The 2010 Deepwater Horizon oil spill incident in the Gulf of Mexico highlighted an urgent need for novel oil-water separation strategies to improve the oil separation effectiveness, which was not achieved with the conventional methods [2]. Commonly, the industrial oily wastewater has been treated with conventional techniques such as adsorption [3], air flotation [4], coagulation [5], centrifugation [6], gravity separation [7-8], and use of an electric field [9]. These techniques need large space, they are also time-consuming, expensive, and contaminant composition dependent while producing a secondary pollutant [2]. Such challenges motivated scientists to develop effective and robust approaches to attain highly efficient oil-water separation [2]. Membrane separation using tailored wettability condition that favors oil separation is among the most studied technology developed for advanced oil-water separation [2]. Superwetting surfaces can provide such a selective filtration of oil or water from an oil-water mixture. For systems comprising of oil and water phases, four wettability states are possible: 1) superhydrophobic and superoleophilic; 2) superhydrophobic and superoleophobic; 3) superhydrophilic and superoleophilic; and 4) superhydrophilic and superoleophobic. These wetting conditions are created by simultaneously modifying surface energy and surface morphology [10].

Depending on the average diameter (d) of the oil droplets, an oil-water mixture can be loosely classified to: free oil ($d > 150$ μm), dispersed oil (20 μm $< d <$ 150 μm), and emulsified oil ($d < 20$ μm) [11]. For

oil-water separation in a gravity-driven process, the membrane is commonly considered to be superhydrophilic and superoleophobic [12-13]. However, there are drawbacks with this wetting condition for dilute oil-in-water contaminations and for high throughput conditions that increase the demand for energy and membrane replacement (due to fouling). In such cases, a large volume of water should be passed through the membrane to separate a relatively smaller volume of oil, increasing pressure drop and the chance of fouling, causing severe permeating flux reduction and decreasing the energy efficiency [14].

To capture oil from oil-water mixtures, various superhydrophobic-superoleophilic (SHSO) surfaces have been designed such as sponges [15-16], papers [17], aerogels [18-19], meshes [20], and mineralized membranes [21]. Recently, stainless steel (SS) mesh-based membranes with SHSO wettability have gained remarkable attention because of their high permeability, low-pressure drop, and high mechanical stability [22-24]. However, there are several limitations with the industrial applications of SHSO membranes. For instance, the fabrication of SHSO surfaces commonly relies on use of complex surface modification methods [25] and fluorinated compounds [26].

The SHSO surfaces are generally constructed by creating a hierarchical micro- and nano-roughness on the surface and modifying the surface chemistry by using low surface energy functional materials [27]. We recently published a comprehensive review paper [24] on the fabrication and characterization of the SHSO membranes with application to oil-water separation. The SHSO SS meshes are widely used in the literature for oil-water separation; however, the oil separation effectiveness is frequently investigated using static tests [11, 23, 26, 28-43]. The first SHSO mesh was fabricated by Feng et al. [44] in 2004 through spray-coating of polytetrafluoroethylene (PTFE) particles (30 wt%) from a solution onto SS mesh, which featured a water contact angle (WCA) of 156° and a sliding angle of 4˚, and a contact angle of zero to oil. Qin et al. [45] used polypropylene sulfide (PPS) in the coating and attained a WCA of 156˚. Yang et al. [38] followed a similar methodology and coated a mesh with epoxy/attapulgite (44.4 wt%). A WCA of

160° and a separation efficiency of 98% after 30 cycles were obtained. Their SHSO mesh showed a high stability under harsh conditions (150 °C and 95% relative humidity for 48 h). Liu et al. [27] constructed a SHSO SiO_2/carbon SS mesh through candle soot coating followed by a chemical vapour deposition. The fabricated membrane with a WCA>150° experienced a high flux of more than 930 $L/m^2 \cdot h$ and oil-water separation efficiency of 97% after 15 process cycles. In our recent study [26], a cross-flow separator set up was designed to measure the static oil-water separation in which over 99% kerosene was effectively separated. We also investigated the effect of silane chain length and solid particle size on the wettability of mesh surfaces [26].

The static oil-water separation tests are mostly conducted by dead-end membranes [17]. To the best of our knowledge, there are only a few studies in the literature that evaluate the performance of continuous oil-water membrane systems with the super wetting surfaces. In the continuous oil-water separation tests, cross-flow membrane systems are used [46], and the hydrodynamics of the fluids make the oil-water separation more challenging compared to the static tests [47]. Dunderdale et al. [25] designed an apparatus using a pair of SS mesh-based membranes, where one as coated with poly(sodium methacrylate) as the water-selective mesh and another coated with poly(stearyl methacrylate) as the oil-selective mesh. They separated oil and water with a purity of near 100% from a 1:1 *n*-hexadecane/water mixture [47]. Ezazi et al. [48] investigated the performance of Fe-TiO_2 spray-coated SS meshes for continuous separation of stabilized oil-in-water emulsions and in-situ photocatalytic degradation of organic matter. The coated mesh showed separation efficiency of over 97%. Moreover, the flux recovery around 99% was observed upon irradiation of visible light on the membrane surface in the continuous separation process [48].

In this research paper, after the introduction section, we report the design and fabrication aspects of a SHSO tubular mesh system for continuous oil-water separation, using free-fall gravity separation. In contrast to typical two-dimensional (2D) filters, the proposed tubular SS mesh with SHSO feature provides more area in a limited space to achieve better oil-water separation efficiency. The effects of

operating conditions including total flow rate and the oil concentration in the inlet on process performance are analyzed. Finally, the designed set-up is used to continuously separate both oil and water phases from an oil-water mixture. The suggested separation methodology can be scaled and has a high potential for implementation in petroleum refining, wastewater treatment, and oil spills clean-up processes.

2 EXPERIMENTAL METHODOLOGY

Materials and Chemicals: 2D SS mesh (316 mesh) is purchased from McMaster-Carr with a nominal opening size of 75 μm. Sulfuric acid (98 wt%, Caledon Laboratory Ltd.), hydrochloric acid (37 wt%, ACP Chemicals), hydrogen peroxide (30 wt%, ACP Chemicals), and acetone (99.5 wt%, ACP Chemicals) are used for cleaning and activation. Long-chain alkyl silane Dynasylan® F8261 and hydrophobic SiO_2 nanoparticles (NPs) AEROSIL® R812 are provided from Evonik Industries AG. All chemicals are used without further purification. Sunflower oil is used to simulate the oil phase in our oil-water separation tests, purchased from a local Canadian Tire supplier. Deionized water (DI, 18.2 MΩ.cm) is obtained by RODI-C-12A, Aqua Solution®. The physical property of the water and oil phases are summarized in Table 1

Table 1. Oil-water mixture properties at ambient temperature at 20˚C.

Fluid	Density ($g.cm^{-3}$)	Kinematic Viscosity ($mm^2.s^{-1}$)
Water	1.00	1
Sunflower oil	0.91	68

Fabrication Process: The general procedure for fabricating the SHSO mesh involves four main steps, including cleaning, activation, coating, and curing. After cleaning the SS mesh tubes with ethanol and acetone in the ultrasound system for 15 min, the activation of cleaned meshes is performed by submerging into piranha solution, a 3:1 volumetric mixture of H_2SO_4 (98 wt%) and H_2O_2 (30 wt). We prepare a prime solution of Dynasylan® F8261 (1 wt%) in ethanol (90 wt%), water (8.8 wt%), and

hydrochloric acid (0.2 wt%). This prime solution is mixed using a magnetic stirrer at 1000 rpm for 2 h. The coating solution is obtained by mixing the prime solution with functionalized silica NPs (1 wt%). The NPs have an average size of 7 nm that are utilized to create a hierarchical nano surface roughness. Subsequently, the coating solution is mixed at 1000 rpm and then ultrasonically dispersed for 30 min. Finally, the dried activated mesh tubes are immersed in the final coating solution to form a stable layer of SHSO onto the mesh tubes. Therefore, the surface energy and morphology of the mesh tubes are modified simultaneously under one-step dip-coating. The coated mesh tubes are allowed to drain excess coating, air dried, and cured at 120˚C for 2 h, and allowed to reach the ambient temperature before being used in the separation tests.

Characterization Methods: The morphology of the SS mesh and SHSO coated mesh is examined by scanning electron microscopy (SEM) using FEI MLA 650 FEG and after gold sputtering. The samples are attached to the surface of an aluminum stub, using a double-side carbon tape. Functionalized fumed silica NPs are also examined using a Tecnai G2 Spirit Transmission Electron Microscopy (TEM), operated at 80 kV. The samples prepared for TEM analysis are diluted in ethanol (95%) and are sonicated for 5 min. For each sample, 5 µl NPs dispersion is applied to a copper grid (300 mesh) coated with carbon, and is then dried at room temperature. The wettability of the as-fabricated SHSO mesh is determined by the equilibrium water and oil contact angle measurements using OCA 15EC (DataPhysics Instruments GmbH, Germany), under ambient conditions. A mesh holder is customized to assure that the mesh stays horizontally, without being stretched, during the contact angle measurements. For each test, 10 µL water droplet is dispensed on the surface of cleaned SHSO meshes; we measure the contact angle of three droplets on different locations on the mesh and repeat the measurements three times (using three independent meshes, and nine droplets in total). For each droplet, the reported contact angle represents the average of both left and right contact angles.

Experimental Set Up and Procedure: The dynamic oil-water separation tests are conducted using a designed set up, as shown in Figure 1. A 1.27 cm SHSO mesh tube (equivalent of ID = ½ inch) is employed to separate the oil from an oil-water mixture under gravity. A ½ inch to ¼ inch Swagelok® reducer stub is used to support the SHSO mesh tube. This mesh is sealed onto the stub using Teflon® shrink tube and a clamp. Also, a 0.63 cm PFA tube (OD = ¼ inch) is attached to the reducer fitting to collect the separated oil in the oil separation vessel. The PFA tube passes through a rubber stopper that is used to seal the bottom of the glass tube with OD=3.1 mm. A sponge cap is used to cover the top of the glass tube to avoid intrusion of dusts, while being open to the atmosphere.

Sunflower oil and DI water are used as the wetting and non-wetting phases, respectively. To remove the air bubbles from the pump head, the outlet stream is vacuumed using a 10 mL disposable syringe before each run. The input oil and water are also de-aerated using a vacuum pump under a vacuum pressure of 22 torr for 5 min. The inlet and outlet of the pumps are connected to the 1/8 and ¼ inch PFA tubes, respectively. After de-aeration, the oil and water are injected into the system at a high flow rate of 20 cm^3/min to ensure that there is no air trapped in the tubes and pump head.

After installing and sealing the separator parts, the glass column is filled with DI water. Due to imperfections in mesh roll welding and to avoid the breakthrough of water, we only allow 3 cm H_2O hydrostatic head relative to the mesh; the height of water column is controlled within a safe margin by adjusting the location of produced water to avoid water breakthrough. The injected oil and water are mixed in a tee connector to create an oil-water mixture. To avoid turbulence around the SHSO mesh tube, the oil-water mixture is added near the oil-air interface. Glass beads with a diameter of 5 mm are used at the bottom of separator to avoid the entrainment of oil droplets along water streamlines near water separation outlet (see Figure 1).

Oil-water mixture with total flow rates (q_t) of 5, 10, and 15 mL/min and oil concentrations of 10, 30, and 50 vol% (e.g., q_o/q_t = 0.1, 0.3, and 0.5) are examined using Eldex pumps for continuous oil and water

co-injection. During the dynamic oil-water separation process, pictures are captured at scheduled timeframes using a digital camera. The entire separation process takes 70 min. We record the collected volumes of water and oil and take pictures at sampling times. The sampling time interval is 2.5 min for the first 10 min and then every 5 min for measurements for the remaining of test duration (10 to 70 min). Using a ruler attached to the outside of the glass tube, the height of oil above the water column is measured.

After each run, vacuum is applied to the separation vessel from bottom to remove the oil from system, including the oil films on mesh. To examine the reproducibility of the results, we repeat each test three times and use a new coated mesh for each replication.

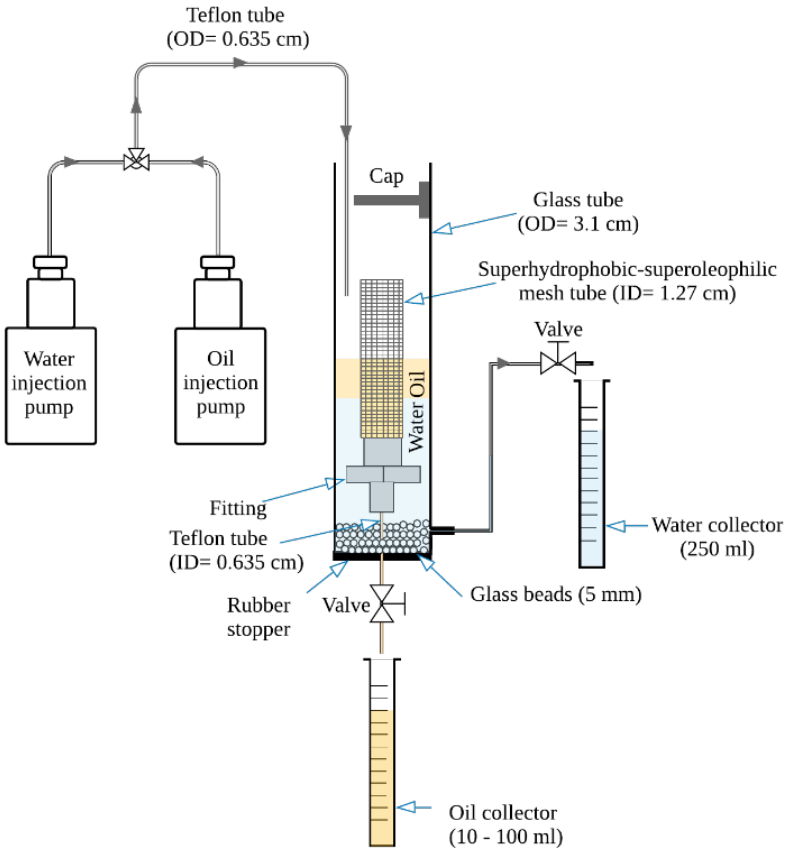

Figure 1: Schematic of dynamic oil-water separation setup.

Experimental Design: In our experiments, a full factorial design (3^k) is implemented where k is the number of factors (e.g., total flow rate and oil in water concentration). For each experimental factor, three levels are tested. Considering a 3^2 design with three replicates, a total of 27 runs are performed as summarized in Table 2. In each experiment, the response variables are the cumulative oil volume, cumulative water volume, and heights of oil and water columns. The raw data are then converted to oil- and water separation efficiency factors.

Table 2. Design of experiments.

Standard runs	Total flow rate (cm^3/min)	Oil concentration at inlet (%)
3		
4		10
5		
18		
19	5	30
21		
2		
16		50
26		
7		
22		10
24		
8		
12	10	30
27		
9		
20		50
25		
1		
10		10
23		
6		
13	15	30
14		
11		
15		50
17		

3 SEPARATION EFFECTIVENESS ANALYSIS

We change the level of oil concentration in the inlet flow and total flow rate of oil-water mixture in the experiments. To analyze the effectiveness of the SHSO mesh tube in separating the oil phase, the collected oil and water volumes are continuously monitored. Having the volumes of original mixture (injected) and collected oil and water samples, the separation efficiency for oil (η_o) is obtained by dividing the collected volume of oil ($V_{c,o}$) to the injected volume of oil ($V_{i,o}$) [27]:

$$\eta_o = \frac{V_{c,o}}{V_{i,o}} \tag{1}$$

Similarly, for the water phase, the separation efficiency (η_w) is obtained by dividing the total collected volume of water to total volume of water injected. The permeate flux of oil (J_o) is given by the following equation:

$$J_o = \frac{V_{c,o}}{S.t} \tag{2}$$

where S is the filtration (active) cross section area for the SHSO mesh in contact with oil; and t represents the separation time. The filtering cross section area S is calculated as follows:

$$S = 2\pi r h \phi \tag{3}$$

where h is the height of oil column in the separator; r stands for the outer radius of the mesh tube; and ϕ introduces the fraction of the membrane area available for flow (2D porosity). Because our membrane is coated, the mesh porosity after coating decreases. The ImageJ. software is employed to calculate the porosity.

The effective membrane resistance (R) to oil permeation can be approximated by the following expression:

$$J_o = \frac{\Delta P - P_c}{\mu R} \approx \frac{\Delta P}{\mu R} \approx \frac{\Delta \rho g h_o}{2\mu R} \tag{4}$$

where ΔP and P_c are the pressure difference across the mesh tube, and capillary pressure respectively; μ is the oil viscosity; $\Delta\rho$ is for the density difference between the oil phase and gas phase (will be approximated by the oil density); and g is the gravity acceleration constant. Because the mesh is superhydrophobic and is completely wetted by the oil phase (superoleophilic), we can neglect the capillary pressure effect as the driving force for oil permeation. Also, at the permeation side, because of complete wetting, the oil phase can flow along the production side of the SHSO mesh and be collected in the oil vessel. The pressure at the permeation side of the membrane is atmospheric. As the height of oil column (h_o) stays nearly constant at steady-state, at the bottom of the oil column, the pressure difference of oil across the membrane is $\Delta\rho g h_o \approx \rho_o g h_o$, while at the top of the oil column, it is zero. Therefore, we can assume the average value as the average driving force for the oil flow across the membrane, and under free-fall gravity conditions.

4 RESULTS AND DISCUSSION

4.1 Superhydrophobic and Superoleophilic Mesh Characterization

We characterize our SHSO SS mesh membranes and examine their stability to acidic, alkaline, and saline solutions as reported in our previous work with details [26]. In this work, the characterization results are given in brief. Figure 2 depicts the SEM images of the cleaned SS mesh and coated SHSO mesh along with the apparent water-air contact angle (WCA) overlay for a 10 μL droplet of DI water on mesh. Figure 2(a) reveals that before coating, the surface of cleaned mesh is neutrally wet with a WCA of 95° at room conditions. As observed in Figure 2(b), after applying the SHSO coating, WCA=163.8° ± 1.8°, showing superhydrophobic characteristic [26]. After the coating process, the contact angle of oil (normal hexane and olive oil) is measured to be zero, implying superoleophilic condition.

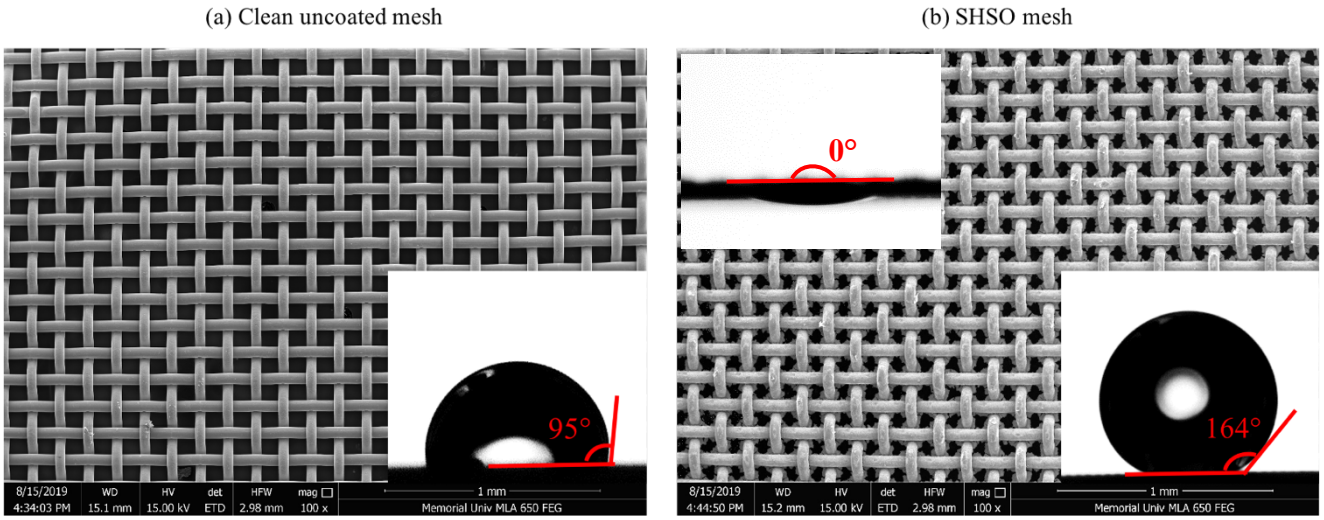

Figure 2: SEM images of (a) cleaned and (b) SHSO coated mesh at 100X magnification, with average contact angles of DI water overlay (bottom-right) and olive oil (top-left).

The mesh nominal pore opening size and the wire mesh woven style affect the surface roughness of the coated mesh as well as the oil-water separation efficiency [44, 49]. Cai et al. [49] noticed that for superhydrophobic woven wire meshes, a WCA>150° can be obtained if the pristine mesh pore diameter is between 50–200 µm. The stainless steel meshes used in this study have a nominal pore size of 75 µm. The pristine mesh wire thickness, pore opening, and porosity are among the design parameters that should be optimized for different systems. Decreasing the wire thickness decreases the overall membrane thickness and consequently pressure drop required for flow of permeate across the membrane. Increasing the pore diameter lowers the viscose pressure drop across the membrane, but also decreases the breakthrough capillary pressure for the water phase to advance into the largest mesh pore, reducing the selectivity of the membrane. When water (as the non-wetting phase) is able to breakthrough, it will be produced along the oil phase and will make membrane less selective by rejecting the water phase. When the oil phase is dispersed, the mesh pore opening should be smaller than the oil droplet characteristic size to be able to capture the droplets upon contact, without allowing the breakthrough of the continuous water phase; however, decreasing the mesh opening increases the resistance to fluid flow.

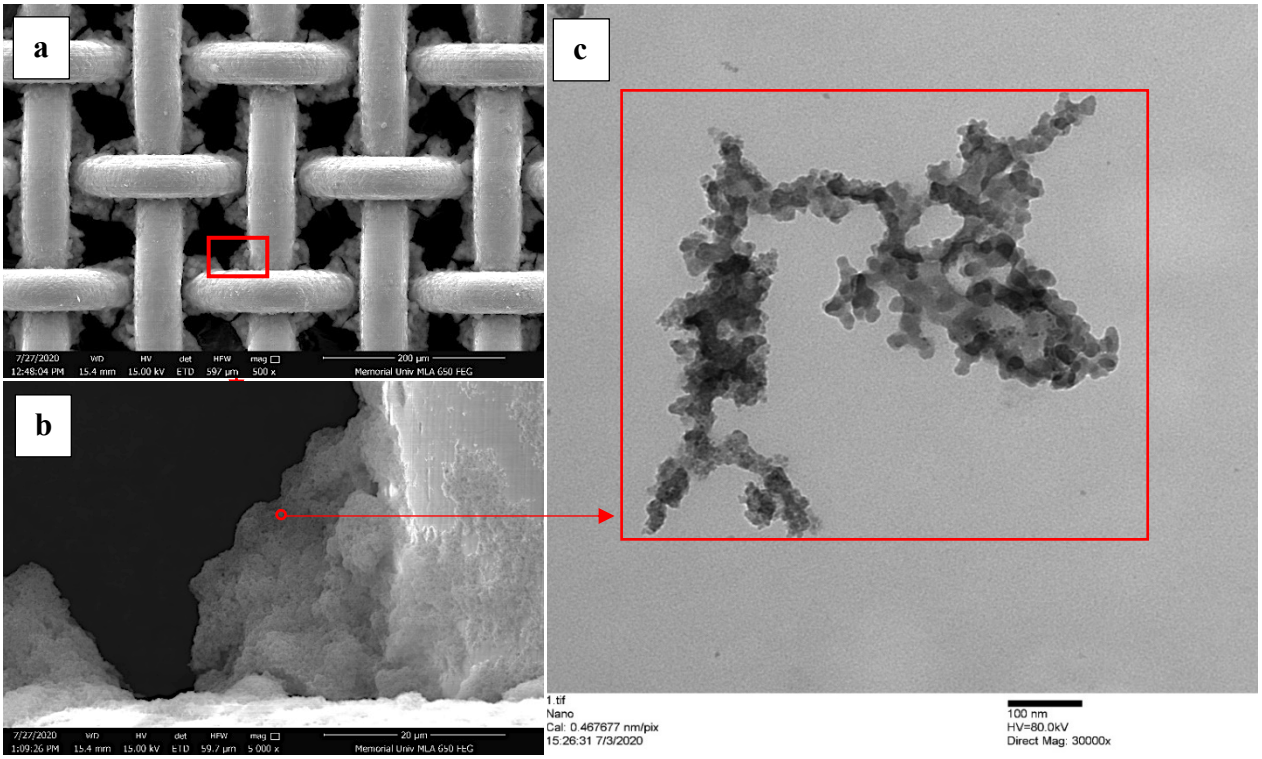

Figure 3: SEM and TEM images of the SHSO mesh; (a) SHSO mesh with 500X magnification and (b) with 5,000X magnification; and (c) the TEM image of functionalized silica NPs as roughness on the surface of mesh with 30,000X magnification.

More details about the coating morphology for the SHSO mesh is given in Figure 3, in which flower-like micro- and nano-scale features can be clearly seen on the surface of the coated mesh. Moreover, the roughness structures with visible fractures in Figure 3(a) provide high capillary pressure regions that can imbibe the oil droplets. The SEM pictures with a higher magnification and 20 µm scale bar is also demonstrated in Figure 3(b); it reveals that the edges of a mesh opening are covered with silica nanoparticles that are bonded to the surface of wires. This creates pore spaces with high capillary pressure that are superhydrophobic and superoleophilic because of the surface roughness and attached fluorocarbon functional groups, which are covalently bonded to the surface of silica nanoparticles. Figure 3(c) shows a TEM image of the silica nanoparticles (AEROSIL® R812) used in the coating solution to create hierarchical micro-and nano-scale surface roughness.

As it is clear from panels (a) and (b) of Figure 3, after the coating, the active cross section area for filtration is reduced due to covalent bonding of functionalized silica nanoparticles to the stainless-steel wire mesh. The reduction in the cross-section porosity after the coating will lower the oil permeation flux (J_o) at a given driving force. To quantify the porosity changes upon coating, we employ SEM pictures of the mesh before and after the coating, as shown in Figure 4(a) and (b), respectively; the ImageJ software is used to determine the reduction in the area available for flow due to the coating. Li's pattern recognition algorithm (in ImageJ auto threshold plugin) is found to fit reasonably well to the open areas of the woven wire mesh, before and after the coating process. A substantial decrease in the porosity is observed from 34.3% to 18.4% due to the coating. From our previous work [26], it was concluded that the breakthrough radius of mesh decreases from (76.4 ± 0.6) μm to (48.3 ± 1.7) μm upon coating.

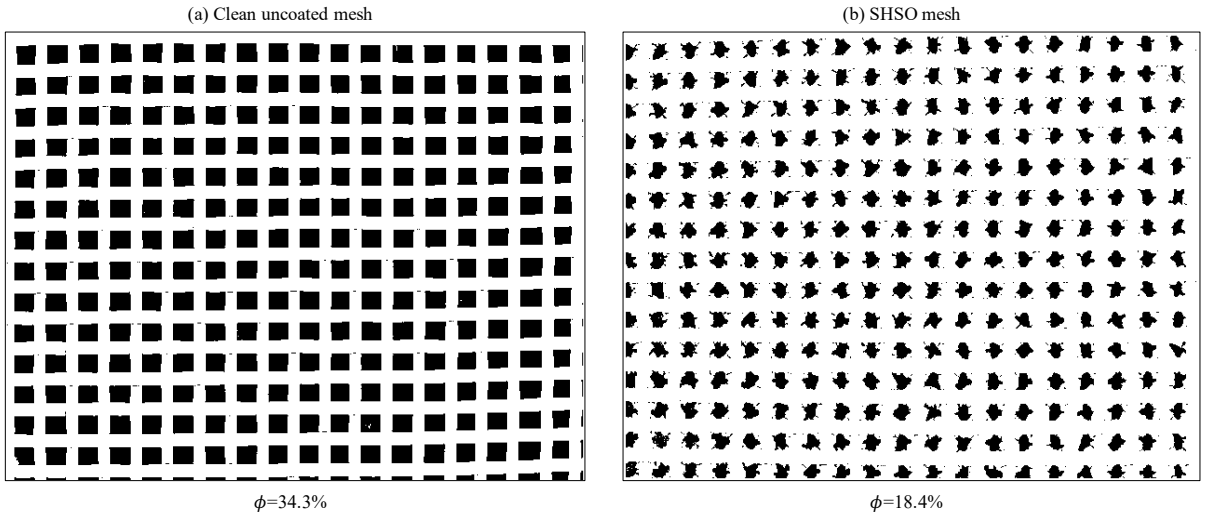

Figure 4: Image processing results to measure the mesh areal porosity for (a) cleaned stainless steel mesh and (b) coated SHSO mesh. The black color indicates pores and the white color represents wire mesh (solid).

4.2. Dynamic Oil-Water Separation Tests

Using the process flow diagram shown in Figure 1, we measure the cumulative volumes of oil and water collected in the graduated cylinders over time. To present the results better, the raw data/variables are

converted to dimensionless numbers. The dimensionless inlet concentration of each phase is obtained by dividing the volumetric flow rate of that specific phase to the total flow rate; at a given time, the collected volume of each phase is divided by total volume injected for that specific phase; and the dimensionless time for collecting each phase is calculated by multiplying time by total flow rate, divided by total injection volume of that given phase. Using these dimensionless numbers, the graphs can be better presented in classified groups as shown in Figure 5, where t and t_f are the injection time and final injection time, respectively. Figure 5 reveals that the introduced dimensionless volume collected linearly correlates with the dimensionless time for both water and oil phases. This observation shows that the oil can be continuously separated upon contact with the SHSO mesh at the same flow rate during the studied injection time. As observed in Figure 5(b), separation of water is not affected by an increase in the total flow rate from 5 to 15 mL/min, and a complete separation is achieved, meaning that at the given flow rate, there is no resistance to the drainage of water. Because the oil phase should pass through the SHSO mesh, which is more confined, a resistance to the oil phase flow is expected as noticed in Figure 5(a). At any given oil inlet concentration (q_o/q_t), as the total flow rate increases, less oil is collected at a given dimensionless time due to the water-oil mixing that decreases the frequency of the oil droplets contacting the SHSO mesh. In addition, Figure 5(a) shows that as the oil concentration at the inlet flow increases at a given total flow rate, the normalized oil volume collected increases. This is because of the SHSO condition and the fact that the volume fraction of oil in the mixing region increases accordingly, accelerating the contact time for the oil droplets with the SHSO mesh, since soon after the oil droplets are brought in contact with the mesh, they can be separated.

(a) oil

(b) water

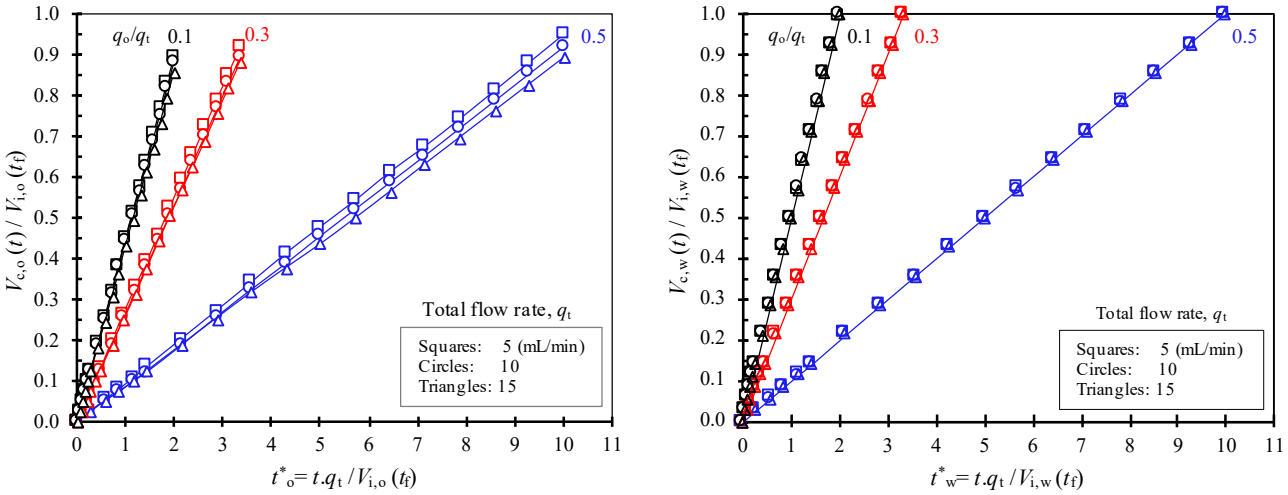

Figure 5: Normalized cumulative volumes of collected fluids vs. dimensionless time for (a) oil and (b) water at different flow rates and oil concentrations at inlet flow stream.

Prior to the discussing results on oil-water separation efficiency, oil permeation flux, membrane resistance, and pressure drop across the membrane, it is logical to analyze the results on the height of oil column in the separator. As shown in Figure 6, the height of oil column in the separator (between the mesh outer surface and glass tube) stays nearly constant over the course of separation, except for the start-up phase. Moreover, increasing the injection flow rate and oil concentration both increase the height of oil column due to the higher resistance for permeation through the SHSO membrane, compared to the drainage of the water phase. In the experiments, the oil is only separated under gravity, and the top of the oil column and the permeate phase are both at the atmospheric conditions.

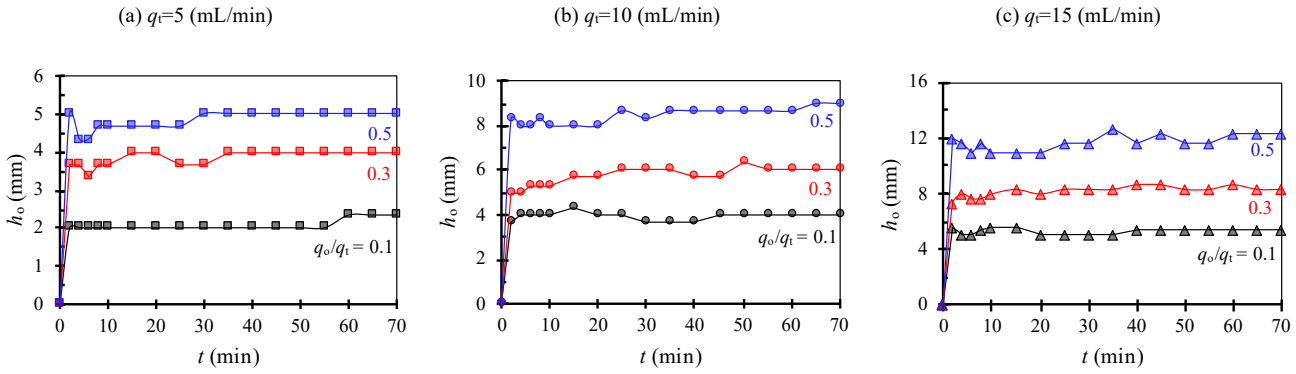

Figure 6: Dynamics of the oil column height in the space between the mesh tube and glass tube at different inlet oil concentrations for total flow rates; (a) 5 mL/min, (b) 10 mL/min, and (c) 15 mL/min.

We use the oil height data as shown in Figure 6. Each run is replicated three times and for each run we take an average value of the height data, after discarding the start-up dynamics for the first 10 min. Thus, after taking the average of the oil column height for the three replicates, the results are shown in Figure 6. The height of oil column can be translated to the maximum pressure driving force across the membrane for oil permeation flux (see Figures 6 and 7). As it is clear from Figure 7(a), by increasing the total injection flow rate (q_t), the maximum pressure driving force across the membrane increases due to more accumulation of oil in the separator as dictated by the membrane resistance. Increasing the volumetric oil concentration at the inlet (q_o / q_t) increases the height of oil column when total injection flow rate is fixed; the main reason is the increased pressure difference for the wetting fluid (oil) across the membrane. At the membrane inner permeation side, the pressure of oil is dictated by the oil-air interface capillary pressure [50]. Because of the oleophilic surface roughness on the mesh wires, the film flow mechanism can help to drain the separated oil. To highlight the effect of water flow rate on the maximum oil pressure driving force across the membrane, Figure 7(b) is plotted in which a linear fit to the total injected oil flow rate is observed. Figure 7(b) shows that the variation in the pressure difference data can be reasonably explained by a linear relationship to the oil flow rate for different injection scenarios. For a better clarity, the error bars are removed. There are some effects from total injection rate as can be seen

for the case of oil injection flow rate 1.5 mL/min; however, the impact of water flow rate along with oil flow rate is minimal in the range of operating conditions tested in this work. The reason for the behavior observed in Figure 7(b) is that the capacity of the separator is dictated by the higher resistance on the permeation side, caused by the smaller pores in the membrane, as opposed to the resistance for water separation. The smaller membrane pores will control permeation through the separator.

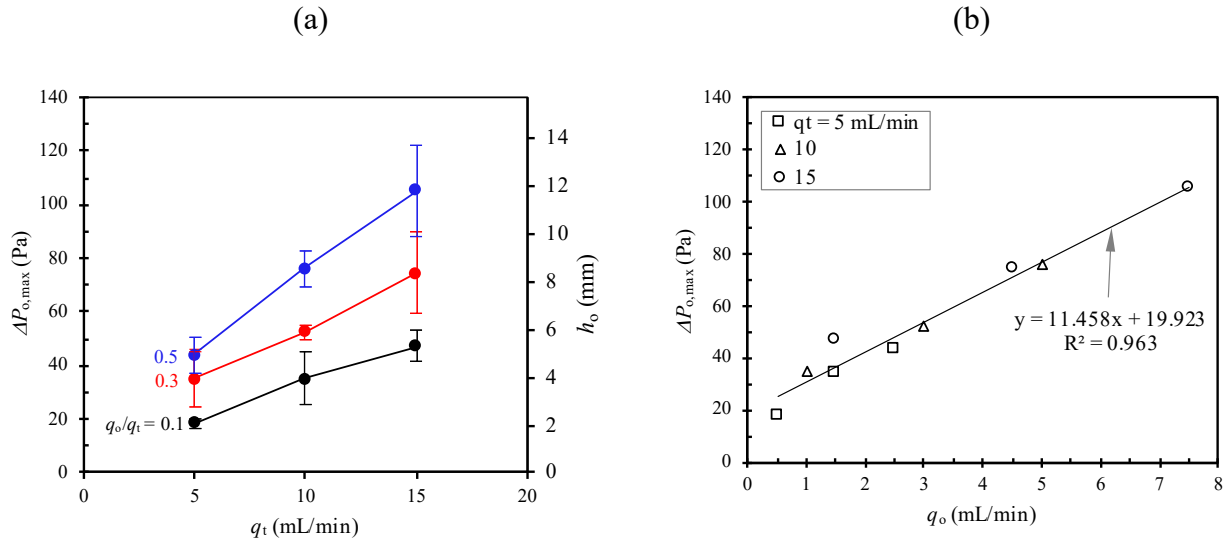

Figure 7: Plots of average height of oil column and maximum hydrostatic pressure driving force for oil permeation vs. (a) total injection flow rate, and (b) oil injection flow rate.

One difficulty with the designed experimental set up is that it does not allow to account for the effect of water dispersion time in the oil column that decreases the contact frequency of oil droplets and membrane.

The oil permeation flux is reported in Figure 8 for different total injection rates. To calculate the oil permeation flux (J_o in Eq. (2)), the collected volume of oil in a given sampling interval is used. Also, we use membrane active (or filtration) area which takes into account the membrane porosity changes after the coating (in Figure 4). The minimum and maximum permeation fluxes for the SHSO membrane operated under gravity separation mechanism are 0.53 L/m^2·s and 1.25 L/m^2·s, respectively. The permeation flux increases as the oil injection flow rate increases according to Figure 8. As observed in

Figures 6 and 7, the increase in the oil injection flow rate also increases the height of oil column, which will in turn increase the driving force for permeation, because we use passive gravity separation, which is one of advantages of the designed separation system. A higher oil flux enables the membrane to handle a larger volume of oil-water mixture in a given time [51]. Also, the oil permeation flux for each injection scenario remains constant during the separation process, implying that the SHSO SS mesh tube exhibits a durable and stable performance upon designed operating conditions [27]. The measured values for the oil permeation flux are comparable to those reported for crossflow filtration [52-55], where the separation process is accelerated by increasing the pressure driving force across the membrane at the cost of higher energy consumption. Another benefit from conducting the test by passive free-fall gravity separation mechanism is that it avoids the breakage of the micro- and nano-roughness features (created in the mesh crevice by the functionalized silica nanoparticles as seen in Figure 3(a)) under high shear conditions). No flux reduction is noticed over 70 min-tests, indicating that the membranes are stable in the range of experimental time. It should be noted that oil flux reduction has been reported in some studies (in the literature) conducted on hydrophobic membranes [54-55].

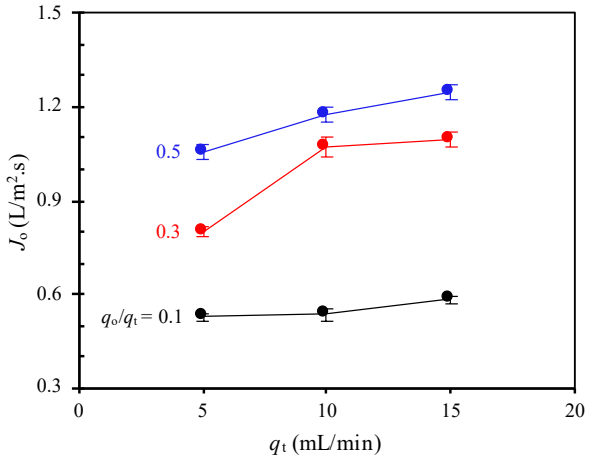

Figure 8: Oil permeation flux vs. total injection rate at different inlet oil concentrations.

From the information on the permeation flux and the height of oil column, the membrane effective resistance (R) can be inferred as shown by Eq. (4). The total effective membrane resistance results are illustrated in Figure 9 for various injection scenarios. As it is clear, the total effective membrane resistance changes between 0.3 and 0.7 (1/μm). The minimum resistance value is obtained at the lowest level of injection flow rate (5 mL/min) and at the minimum oil concentration in the inlet flow (10%). The maximum resistance value is attained at the highest injection flow rate (15 mL/min) and at the highest oil concentration in the inlet (50%). The large variability in the height of oil column (see Figure 6(a)) belongs to the case of 5 mL/min at 30% inlet oil volume, which makes the membrane resistance at this scenario slightly higher than the case of 50% oil concentration as expected.

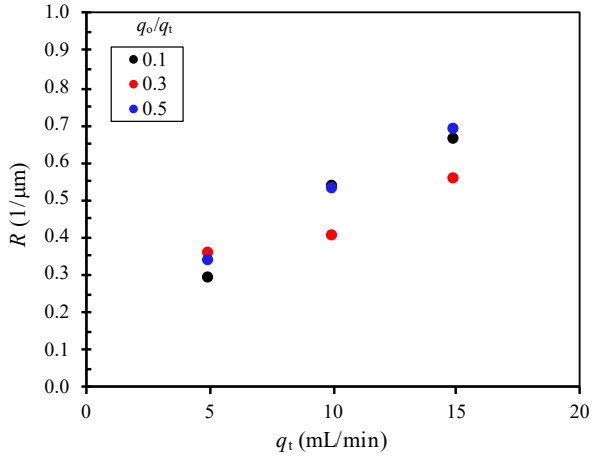

Figure 9: Total membrane resistance as a function of total injection flow rate at different inlet oil concentrations.

To better evaluate the separation performance of the fabricated SHSO mesh, the separation efficiency for the oil and water phases are calculated over time for different scenarios, using the injected and collected oil and water volumes (see Eq. (1)). All tests are repeated three times, and the reported results are the averaged values. The dynamics of oil-water separation efficiency for the oil and water phases is depicted in Figure 10. The left side panels (Figure 10(a)) show the separation efficiency for oil at different injection flow rates q_t=5, 10, and 15 mL/min, and the right-side panels (Figure 10(b)) report

the separation efficiency for water at these three levels of total injection rates. For a better clarity, the error bars are not shown, and the results only represent one set of the tests. According to Figure 10(a), the oil separation efficiency (η_o) reaches a stable separation efficiency within 55 min injection, which is stabilized faster at lower injection rates. Also, a higher separation efficiency for oil is obtained at lower oil injection rates. The maximum separation efficiency for oil is achieved at 5 mL/min, and 10% inlet oil concentration is observed with an average value of 95.6% ± 1.2% (for three replicates). As expected, the minimum oil separation efficiency happens for the maximum oil inlet flow rate (case of 15 mL/min at 50% oil inlet concentration) at an average value of 85.4% ± 1.8% (for three replicates). For the specific run shown in Figure 10(a), at the lowest total injection rate (5 mL/min), the oil separation efficiencies are 97%, 90% and 90% for the inlet oil concentrations of 10%, 30%, and 50%, respectively. It should be emphasized that the oil separation efficiency of 90% means that 90% of the oil can be continuously separated at steady state condition. As discussed in Figure 6(b), by increasing the oil injection flow rate, the height of oil column increases. Therefore, a part of the injected oil will stay in the mixing zone to maintain the higher oil height, as an interplay between the injection and permeation. It does not mean that for a case of 90% separation efficiency, the remaining of oil cannot be separated. From our previous static tests, at the end of experiments and when the injection is stopped, an ultimate separation of >99% can be reached by allowing enough time [26]. To obtain the same separation efficiency when the oil injection rate increases, a longer residence time is required for separation, which can be obtained by increasing the SHSO mesh active filtration surface area. Although the mean values for the oil separation efficiency are reduced with increasing the oil concentration as shown in Figure 10(a), the differences (given three replicates) are not statistically significant at 95% confidence level for some cases. We will show this overlap, especially for the case of mid-level flow rate later.

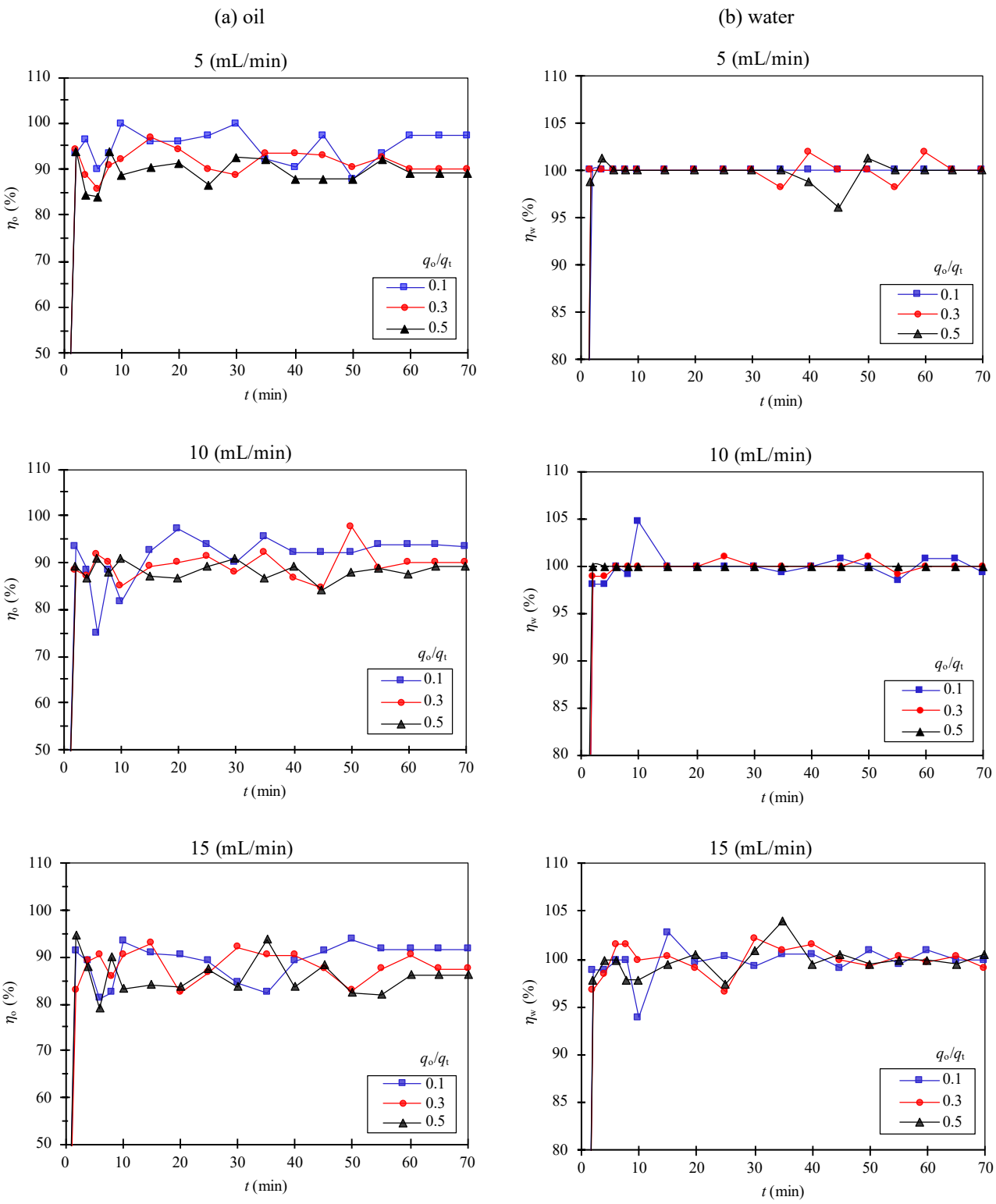

Figure 10: Dynamics of oil-water separation efficiency using SHSO mesh membrane for: (a) oil and (b) water at different injection scenarios.

Unlike oil separation efficiency, the water separation efficiency (η_w) is not affected by the flow rate of oil or total flow rate according to Figure 10(b), in which the water separation efficiency stays near 100% for all injection scenarios.

In Figure 11, a summary of the averaged separation efficiencies for the oil and water phases are displayed. In each run, the separation efficiency is averaged for the period 10–70 min to remove the dynamic effects of the experiment start up. The reported separation efficiency values are the average of three replicates, and the error bars for the oil show 95% confidence intervals. As observed in Figure 11(a), the oil separation efficiency decreases with increasing the oil flow rate. A decrease in the oil separation efficiency upon an increase in the oil flow rate is due to the increased height of oil accumulation in the column, which demands a part of the injected oil to be always trapped in the mixing zone. To achieve the same separation efficiency at various flow rates, the ratio of inlet flow rate of oil to mesh active surface area should be scaled. According to Figure 11(a), differences between the means of separation efficiency are significant for the lowest and highest levels of total injection flow rate (5 mL/min and 15 mL/min); however, there are some overlaps between the error bars when differences between the means for the mid-level flow rate (10 mL/min) and other two flow rates are considered, implying that the difference might not be statistically significant.

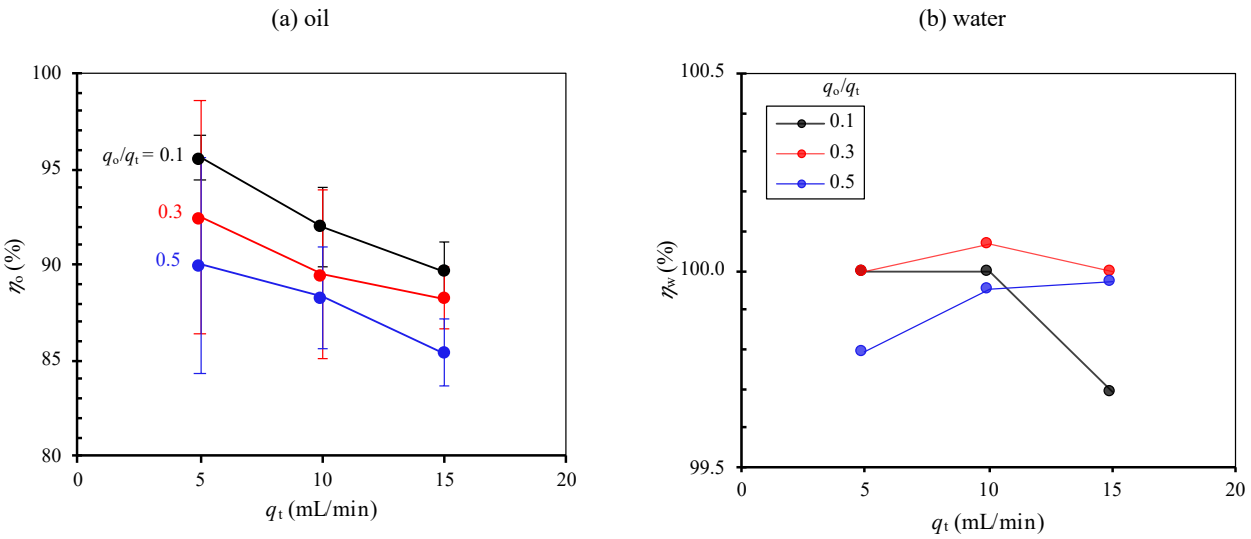

Figure 11: A summary of average separation efficiencies for (a) oil and (b) water at different injection flow rates and inlet oil concentrations. The values are averaged for three replicates and the error bars show 95% confidence interval.

As illustrated in Figure 11(b), the separation efficiency for water (η_w) is practically near 100% for most cases, and the deviations from 100% are due to the experimental errors.

In Table 3, we summarize average experimental result values, including the averaged values for the oil flux, the maximum pressure difference of oil phase across the membrane, oil separation efficiency, water separation efficiency, and membrane effective resistance at different injection scenarios. For each run, the average values are taken, after discarding the data for the first 10 min to eliminate the dynamics effects related to the start up. Then, 95% confidence interval around the sample means with three replicates are considered in Table 3.

Table 3. A summary of separation performance. The values are the average of three runs, and for each run the point estimates are the average for the period 10-70 min.

q_t (mL/min)	q_o/q_t	$\Delta P_{o,max} = \Delta\rho_o g h_o$ (Pa)	J_o (L/m^2·s)	η_o	η_w	R (1/μm)
5	0.1	18.6 ± 1.8	0.526 ± 0.015	95.6 ± 1.2	100.0 ± 0.0	0.286 ± 0.029
	0.3	35.0 ± 10.7	0.800 ± 0.017	92.5 ± 6.1	100.0 ± 0.3	0.354 ± 0.108
	0.5	43.9 ± 6.8	1.056 ± 0.024	90.0 ± 5.6	99.8 ± 0.4	0.336 ± 0.053
10	0.1	35.3 ± 9.7	0.533 ± 0.020	92.0 ± 2.1	100.0 ± 0.0	0.535 ± 0.148
	0.3	52.7 ± 2.6	1.072 ± 0.032	89.5 ± 4.4	100.0 ± 0.3	0.397 ± 0.0.0
	0.5	76.2 ± 6.8	1.176 ± 0.027	88.3 ± 2.7	100.0 ± 0.6	0.524 ± 0.048
15	0.1	47.3 ± 6.0	0.581 ± 0.012	90.0 ± 5.6	99.7 ± 1.3	0.658 ± 0.084
	0.3	74.6 ± 15.5	1.099 ± 0.024	88.3 ± 2.7	100.0 ± 0.0	0.549 ± 0.114
	0.5	105.2 ± 17.1	1.248 ± 0.0237	85.4 ± 1.8	100.0 ± 0.6	0.681 ± 0.111

5 PRACTICAL IMPLICATIONS AND CHALLENGES

Unlike some studies that use pair of water-selective and oil-selective membranes, we propose a simple and efficient methodology that uses one SHSO membrane. Also, we avoid cross-flow filtration, which is expected to improve the membrane lifetime because of decreased shear that can potentially break the high capillary pressure of flower-like rough pore spaces. The proposed methodology uses simple and passive gravity separation and is scalable. The suggested method is useful for separation of dispersed or free-oil, and combines gravity settling and membrane separation. As only the oil layer is needed to be in contact with the SHSO membrane, less membrane surface area is required. The methodology is energy efficient for the case of dilute oil contaminations where the majority of mixture is water. One potential benefit of the proposed methodology is using SHSO membrane and gravity settling. Thus, it is expected that water-based fouling damages the membrane much less because water cannot wet the membrane and only oil is permeated through the membrane and water is allowed to settle. More research is required to study the performance of our SHSO membrane system in the presence of water- and oil-based fouling. Although applying controlled vacuum to the oil collection vessel can facilitate the oil flux, it is expensive, and will increase the chance for water breakthrough.

There are potentially three critical challenges that can limit the performance of our SHSO membrane separation system. The most important challenge is related to the presence of surfactant in oil-water mixture. Because the SHSO relies on the capillary pressure contrast of water and oil phases, the presence of surfactant will decrease the membrane selectivity, by allowing water phase to break through. The next challenge is emulsified oil-in-water contaminations. The small size of oil droplets limits the choice of SS mesh size as the pore openings should be smaller than the characteristic emulsion size, and for fine emulsions, this causes increased membrane resistance. The third important challenge is the presence of viscous oil contaminations, which require higher pressure differences for the permeate across membrane, limiting oil flux. For example, this can be an issue for the separation of oil spills in cold environment, such as the Arctic. In general, the membrane characteristics should be optimized based on operating conditions.

6 CONCLUSIONS

In this study, the SHSO mesh tube is employed in a vertical cross-flow filtration set up to continuously separate oil-water mixtures with different oil concentrations (10, 30, and 50 vol%) and total flow rates (5, 10, and 15 cm^3/min). A SS mesh tube is activated with a piranha solution; the surface chemistry and morphology of the mesh are then modified to obtain SHSO condition by dip-coating into a solution containing DYNASYLAN® F8261, ethanol, water, hydrochloric acid, and functionalized NPs. We use hexamethyldisilazane (HMDS) modified fumed silica with average sizes of 10 nm to create a hierarchical nano roughness. To study the performance of the dynamic experimental set up, a tubular SHSO membrane with 10.5 cm height and an effective surface area of 0.3-1.8 cm^2 is used. The following key conclusions are drawn from this study:

- According to the SEM images, the flower-like nano roughness not only provides an extended surface area with an effective water-repellency feature, but it also creates regions with high

capillary pressure that favorably pass through the oil phase. The mesh pore opening of 80 and 45 μm are obtained for the original and coated mesh, respectively.

- Compared to the cleaned mesh with a WCA of > 90°, the as-fabricated SHSO mesh demonstrates a WCA of 160°, which is above the value of 150° defined for the superhydrophobic surfaces. The sunflower oil completely wets the surface of the coated mesh, revealing the SHSO characteristic of the as-fabricated mesh.
- The cumulative amount of produced oil and water shows a linear behavior over the separation process. This implies that there is no blockage in the membrane pores under different oil concentration and total flow rate conditions.
- A reduction in oil SE is observed upon an increase in total flow rate (5 to 15 cm^3/min) and oil concentration (10–50 vol%). The case with 5 cm^3/min total flow rate and 10 vol% oil concentration leads to a maximum oil SE of 97%. In contrary, a minimum oil SE (86%) is obtained when the injection flow rate of oil-water mixture is 15 cm^3/min, and the oil concentration is 50 vol%.
- The water SE attains almost 100% in the designed experiments. This implies that the SE of water phase is not affected by the total flow rate and oil concentration.
- The SHSO membrane experiences high permeation flux of oil phase (314–790 $L/m^2 \cdot h$) when the total flow rate is increased from 5 to 15 mL/min; in other words, the inlet oil flow rate is increased from 0.5–7.5 cm^3/min.
- This permeate flux is controlled by membrane permeability. Thus, increasing the inlet oil flow beyond the maximum possible flow rate results in accumulation of the oil phase around the mesh.
- The oil-water separation process through SHSO membranes can be modified for larger scales. We can extend the surface area by adding more SHSO mesh tubes. Reusing the non-fouling SHSO membranes can lower the costs of oily wastewater treatment processes. Thus, there is a

high potential of using the proposed separation strategy in petroleum refining, wastewater treatment, and oil spills clean-up processes.

ACKNOWLEDGEMENTS

The authors would like to thank the Natural Sciences and Engineering Research Council of Canada (NSERC), InnovateNL, Suncor Energy, and Memorial University for the financial support of this project.

DISCLOSURE

This manuscript is a part of the master thesis of the first author (Seyedabbas Rasouli) in Memorial University (MUN), Canada. In fact, the graduate students in MUN can submit their thesis either in a traditional way or manuscript base. In the latter case, each chapter (manuscript) might have been published or submitted at the time of thesis submission. This is acknowledged in the thesis and contributions of all co-authors are clearly mentioned in the thesis. Thus, it is confirmed that the authors follow the MUN thesis regulations/guidelines of manuscript style and there is no issue with the copyright.

NOMENCLATURES

Acronyms

DOE	-	Design of experiment
DI	-	Deionized
ID		Inner diameter

NPs	-	Nanoparticles
OCA		Oil contact angle
OD		Outer diameter
PPS	-	Polypropylene sulfide
PTFE	-	Polytetrafluoroethylene
rpm	-	Rate per minute
SEM	-	Scanning electron microscopy
SHSO	-	Superhydrophobic-Superoleophilic
SS	-	Stainless steel
TEM	-	Transmission Electron Microscopy
WCA	-	Water contact angle

Variables/Symbols

g	Gravitational acceleration	($m.s^{-2}$)
h	Height of fluids in the column	(m)
h_o	Height of oil in the column	(m)
J_o	Oil permeation flux	($m^3.m^{-2}.s^{-1}$)
P	Liquid pressure	(Pa)
P_c	Capillary pressure	(Pa)
q_o	Oil injection flow rate	($m^3.s^{-1}$)
q_t	Total injection flow rate	($m^3.s^{-1}$)
q_w	Water injection flow rate	($m^3.s^{-1}$)
R	Membrane effective resistance	(m^{-1})

r	Outer radius of mesh tube	(m)
S	Active filtration area	(m^2)
t	Time	(s)
t_f	Final injection time	(s)
$V_{c,o}$	Cumulative volume of oil collected (filtered)	(m^3)
$V_{c,w}$	Cumulative volume of water collected	(m^3)
$V_{i,o}$	Cumulative volume of oil injected	(m^3)
$V_{i,w}$	Cumulative volume of water	(m^3)

Greek Letters

ΔP	Pressure difference for the wetting phase across membrane	(Pa)
$\Delta P_{o,max}$	Maximum hydrostatic height difference for wetting phase	(Pa)
$\Delta\rho$	Density difference between oil and air	($kg.m^{-3}$)
η_o	Oil separation efficiency	($m^3.m^{-3}$)
η_o	Oil separation efficiency	($m^3.m^{-3}$)
η_w	Water separation efficiency	($m^3.m^{-3}$)
μ	Viscosity	($Pa.m^{-1}.s^{-1}$)
ϕ	Mesh 2D porosity	($m^2.m^{-2}$)

REFERENCES

1. Liu, N.; Zhang, Q.; Qu, R.; Zhang, W.; Li, H.; Wei, Y.; Feng, L., Nanocomposite Deposited Membrane for Oil-in-Water Emulsion Separation with in Situ Removal of Anionic Dyes and Surfactants. *Langmuir* **2017,** *33* (30), 7380-7388.
2. Deng, D.; Prendergast, D. P.; Macfarlane, J.; Bagatin, R.; Stellacci, F.; Gschwend, P. M., Hydrophobic meshes for oil spill recovery devices. *ACS applied materials & interfaces* **2013,** *5* (3), 774-781.

3. Diaz de Tuesta, J. L.; Silva, A. M. T.; Faria, J. L.; Gomes, H. T., Removal of Sudan IV from a simulated biphasic oily wastewater by using lipophilic carbon adsorbents. *Chemical Engineering Journal* **2018,** *347*, 963-971.
4. Rocha e Silva, F. C. P.; Rocha e Silva, N. M. P.; da Silva, I. A.; Ferreira Brasileiro, P. P.; Luna, J. M.; Rufino, R. D.; Santos, V. A.; Sarubbo, L. A., Oil removal efficiency forecast of a Dissolved Air Flotation (DAF) reduced scale prototype using the dimensionless number of Damköhler. *Journal of Water Process Engineering* **2018,** *23*, 45-49.
5. Teh, C. Y.; Budiman, P. M.; Shak, K. P. Y.; Wu, T. Y., Recent Advancement of Coagulation–Flocculation and Its Application in Wastewater Treatment. *Industrial & Engineering Chemistry Research* **2016,** *55* (16), 4363-4389.
6. Liu, M.; Chen, J.; Cai, X.; Han, Y.; Xiong, S., Oil–water pre-separation with a novel axial hydrocyclone. *Chinese Journal of Chemical Engineering* **2018,** *26* (1), 60-66.
7. Abdurahman H. Nour, F. S. M., Rosli M. Yunus and A. Arman, , Demulsification of Virgin Coconut Oil by Centrifugation Method: A Feasibility Study. *International Journal of Chemical Technology* **2009,** *1* (2), 59-64.
8. Saththasivam, J.; Loganathan, K.; Sarp, S., An overview of oil–water separation using gas flotation systems. *Chemosphere* **2016,** *144*, 671-680.
9. Kwon, W.-T.; Park, K.; Han, S. D.; Yoon, S. M.; Kim, J. Y.; Bae, W.; Rhee, Y. W., Investigation of water separation from water-in-oil emulsion using electric field. *Journal of Industrial and Engineering Chemistry* **2010,** *16* (5), 684-687.
10. Brown, P. S.; Bhushan, B., Bioinspired, roughness-induced, water and oil super-philic and super-phobic coatings prepared by adaptable layer-by-layer technique. *Scientific reports* **2015,** *5*, 14030.
11. Feng, L.; Zhang, Z.; Mai, Z.; Ma, Y.; Liu, B.; Jiang, L.; Zhu, D., A Super-Hydrophobic and Super-Oleophilic Coating Mesh Film for the Separation of Oil and Water. *Angewandte Chemie* **2004,** *116* (15), 2046-2048.
12. Lin, L.; Liu, M.; Chen, L.; Chen, P.; Ma, J.; Han, D.; Jiang, L., Bio-Inspired Hierarchical Macromolecule–Nanoclay Hydrogels for Robust Underwater Superoleophobicity. *Advanced materials (Weinheim)* **2010,** *22* (43), 4826-4830.
13. Sun, T.; Feng, L.; Gao, X.; Jiang, L., Bioinspired Surfaces with Special Wettability. *Accounts of chemical research* **2005,** *38* (8), 644-652.
14. Yan, L.; Yang, X.; Zeng, H.; Zhao, Y.; Li, Y.; He, X.; Ma, J.; Shao, L., Nanocomposite hydrogel engineered hierarchical membranes for efficient oil/water separation and heavy metal removal. *J. Membr. Sci.* **2023,** *668*, 121243.
15. He, Z.; Wu, H.; Shi, Z.; Kong, Z.; Ma, S.; Sun, Y.; Liu, X. Facile Preparation of Robust Superhydrophobic/Superoleophilic TiO₂-Decorated Polyvinyl Alcohol Sponge for Efficient Oil/Water Separation *ACS Omega* [Online], 2022, p. 7084-7095. PubMed.
16. Ke, Q.; Jin, Y.; Jiang, P.; Yu, J., Oil/Water Separation Performances of Superhydrophobic and Superoleophilic Sponges. *Langmuir* **2014,** *30* (44), 13137-13142.
17. He, Z.; Wu, H.; Shi, Z.; Gao, X.; Sun, Y.; Liu, X., Mussel-Inspired Durable TiO2/PDA-Based Superhydrophobic Paper with Excellent Self-Cleaning, High Chemical Stability, and Efficient Oil/Water Separation Properties. *Langmuir* **2022,** *38* (19), 6086-6098.
18. Wang, N.-N.; Wang, H.; Wang, Y.-Y.; Wei, Y.-H.; Si, J.-Y.; Yuen, A. C. Y.; Xie, J.-S.; Yu, B.; Zhu, S.-E.; Lu, H.-D.; Yang, W.; Chan, Q. N.; Yeoh, G.-H., Robust, Lightweight, Hydrophobic, and Fire-Retarded Polyimide/MXene Aerogels for Effective Oil/Water Separation. *ACS Applied Materials & Interfaces* **2019,** *11* (43), 40512-40523.
19. Shi, G.; Wu, M.; Zhong, Q.; Mu, P.; Li, J., Superhydrophobic Waste Cardboard Aerogels as Effective and Reusable Oil Absorbents. *Langmuir* **2021,** *37* (25), 7843-7850.
20. Liu, M.; Hou, Y.; Li, J.; Guo, Z., Stable Superwetting Meshes for On-Demand Separation of Immiscible Oil/Water Mixtures and Emulsions. *Langmuir* **2017,** *33* (15), 3702-3710.
21. Li, Y.; Yang, X.; Wen, Y.; Zhao, Y.; Yan, L.; Han, G.; Shao, L., Progress reports of mineralized membranes: Engineering strategies and multifunctional applications. *Sep. Purif. Technol.* **2023,** *304*, 122379.

22. Liu, Y.; Liu, F.; Ni, L.; Meng, M.; Meng, X.; Zhong, G.; Qiu, J., A modeling study by response surface methodology (RSM) on Sr(ii) ion dynamic adsorption optimization using a novel magnetic ion imprinted polymer. *RSC Advances* **2016,** *6* (60), 54679-54692.
23. Zhang, Y.; Wang, X.; Wang, C.; Liu, J.; Zhai, H.; Liu, B.; Zhao, X.; Fang, D., Facile fabrication of zinc oxide coated superhydrophobic and superoleophilic meshes for efficient oil/water separation. *RSC Advances* **2018,** *8* (61), 35150-35156.
24. Rasouli, S.; Rezaei, N.; Hamedi, H.; Zendehboudi, S.; Duan, X., Superhydrophobic and superoleophilic membranes for oil-water separation application: A comprehensive review. *Materials & Design* **2021,** *204*, 109599.
25. Dunderdale, G. J.; Urata, C.; Sato, T.; England, M. W.; Hozumi, A., Continuous, High-Speed, and Efficient Oil/Water Separation using Meshes with Antagonistic Wetting Properties. *ACS applied materials & interfaces* **2015,** *7* (34), 18915-18919.
26. Rasouli, S.; Rezaei, N.; Hamedi, H.; Zendehboudi, S.; Duan, X., Design, fabrication, and characterization of a facile superhydrophobic and superoleophilic mesh-based membrane for selective oil-water separation. *Chem. Eng. Sci.* **2021,** *236*, 116354.
27. Liu, D.; Yu, Y.; Chen, X.; Zheng, Y., Selective separation of oil and water with special wettability mesh membranes. *RSC Advances* **2017,** *7* (21), 12908-12915.
28. Xiang, M.; Jiang, M.; Zhang, Y.; Liu, Y.; Shen, F.; Yang, G.; He, Y.; Wang, L.; Zhang, X.; Deng, S., Fabrication of a novel superhydrophobic and superoleophilic surface by one-step electrodeposition method for continuous oil/water separation. *Applied Surface Science* **2018,** *434*, 1015-1020.
29. Lee, C.; Baik, S., Vertically-aligned carbon nano-tube membrane filters with superhydrophobicity and superoleophilicity. *Carbon* **2010,** *48* (8), 2192-2197.
30. Wang, C.-F.; Tzeng, F.-S.; Chen, H.-G.; Chang, C.-J., Ultraviolet-Durable Superhydrophobic Zinc Oxide-Coated Mesh Films for Surface and Underwater–Oil Capture and Transportation. *Langmuir* **2012,** *28* (26), 10015-10019.
31. Wang, S.; Li, M.; Lu, Q., Filter Paper with Selective Absorption and Separation of Liquids that Differ in Surface Tension. *ACS Applied Materials & Interfaces* **2010,** *2* (3), 677-683.
32. Yang, H.; Pi, P.; Cai, Z.-Q.; Wen, X.; Wang, X.; Cheng, J.; Yang, Z.-r., Facile preparation of super-hydrophobic and super-oleophilic silica film on stainless steel mesh via sol–gel process. *Applied Surface Science* **2010,** *256* (13), 4095-4102.
33. Yang, H.; Zhang, X.; Cai, Z.-Q.; Pi, P.; Zheng, D.; Wen, X.; Cheng, J.; Yang, Z.-r., Functional silica film on stainless steel mesh with tunable wettability. *Surface and Coatings Technology* **2011,** *205* (23), 5387-5393.
34. Li, H.; Zheng, M.; Ma, L.; Zhu, C.; Lu, S., Two-dimensional ZnO nanoflakes coated mesh for the separation of water and oil. *Materials Research Bulletin* **2013,** *48* (1), 25-29.
35. Liu, Y.; Zhang, K.; Yao, W.; Liu, J.; Han, Z.; Ren, L., Bioinspired structured superhydrophobic and superoleophilic stainless steel mesh for efficient oil-water separation. *Colloids and Surfaces A: Physicochemical and Engineering Aspects* **2016,** *500*, 54-63.
36. Matin, A.; Baig, U.; Gondal, M. A.; Akhtar, S.; Zubair, S. M., Superhydrophobic and superoleophilic surfaces prepared by spray-coating of facile synthesized Cerium(IV) oxide nanoparticles for efficient oil/water separation. *Applied Surface Science* **2018,** *462*, 95-104.
37. Baig, U.; Matin, A.; Gondal, M. A.; Zubair, S. M., Facile fabrication of superhydrophobic, superoleophilic photocatalytic membrane for efficient oil-water separation and removal of hazardous organic pollutants. *Journal of Cleaner Production* **2019,** *208*, 904-915.
38. Yang, J.; Tang, Y.; Xu, J.; Chen, B.; Tang, H.; Li, C., Durable superhydrophobic/superoleophilic epoxy/attapulgite nanocomposite coatings for oil/water separation. *Surface and Coatings Technology* **2015,** *272*, 285-290.
39. Li, J.; Guan, P.; Zhang, Y.; Xiang, B.; Tang, X.; She, H., A diatomite coated mesh with switchable wettability for on-demand oil/water separation and methylene blue adsorption. *Separation and Purification Technology* **2017,** *174*, 275-281.
40. Cao, W.-T.; Liu, Y.-J.; Ma, M.-G.; Zhu, J.-F., Facile preparation of robust and superhydrophobic materials for self-cleaning and oil/water separation. *Colloids and Surfaces A: Physicochemical and Engineering Aspects* **2017,** *529*, 18-25.

41. Xiao, C.; Si, L.; Liu, Y.; Guan, G.; Wu, D.; Wang, Z.; Hao, X., Ultrastable coaxial cable-like superhydrophobic mesh with self-adaption effect: facile synthesis and oil/water separation application. *Journal of Materials Chemistry A* **2016,** *4* (21), 8080-8090.
42. Matin, A.; Baig, U.; Gondal, M. A.; Akhtar, S.; Zubair, S. M., Facile fabrication of superhydrophobic/superoleophilic microporous membranes by spray-coating ytterbium oxide particles for efficient oil-water separation. *Journal of Membrane Science* **2018,** *548*, 390-397.
43. Du, Z.; Ding, P.; Tai, X.; Pan, Z.; Yang, H., Facile Preparation of Ag-Coated Superhydrophobic/Superoleophilic Mesh for Efficient Oil/Water Separation with Excellent Corrosion Resistance. *Langmuir* **2018,** *34* (23), 6922-6929.
44. Feng, L.; Zhang, Z.; Mai, Z.; Ma, Y.; Liu, B.; Jiang, L.; Zhu, D., A Super-Hydrophobic and Super-Oleophilic Coating Mesh Film for the Separation of Oil and Water. *Angewandte Chemie International Edition* **2004,** *43* (15), 2012-2014.
45. Qin, F.; Yu, Z.; Fang, X.; Liu, X.; Sun, X., A novel composite coating mesh film for oil-water separation. *Frontiers of Chemical Engineering in China* **2009,** *3* (1), 112-118.
46. Xiong, Z.; Lin, H.; Liu, F.; Xiao, P.; Wu, Z.; Li, T.; Li, D., Flexible PVDF membranes with exceptional robust superwetting surface for continuous separation of oil/water emulsions. *Scientific reports* **2017,** *7* (1), 14099-12.
47. Binner, E. R.; Robinson, J. P.; Kingman, S. W.; Lester, E. H.; Azzopardi, B. J.; Dimitrakis, G.; Briggs, J., Separation of Oil/Water Emulsions in Continuous Flow Using Microwave Heating. *Energy & Fuels* **2013,** *27* (6), 3173-3178.
48. Ezazi, M.; Shrestha, B.; Kim, S. I.; Jeong, B.; Gorney, J.; Hutchison, K.; Lee, D. H.; Kwon, G., Selective Wettability Membrane for Continuous Oil−Water Separation and In Situ Visible Light-Driven Photocatalytic Purification of Water. *Global challenges* **2020,** *4* (10), 2000009-n/a.
49. Cai, Y.; Li, S.; Cheng, Z.; Xu, G.; Quan, X.; Zhou, Y., Facile fabrication of super-hydrophobic FAS modified electroless Ni-P coating meshes for rapid water-oil separation. *Colloids and Surfaces A: Physicochemical and Engineering Aspects* **2018,** *540*, 224-232.
50. Mruetusatorn, P.; Polizos, G.; Datskos, P. G.; Taylor, G.; Sarles, S. A.; Boreyko, J. B.; Hayes, D. G.; Collier, C. P., Control of Membrane Permeability in Air-Stable Droplet Interface Bilayers. *Langmuir* **2015,** *31* (14), 4224-4231.
51. He, S.; Zhan, Y.; Bai, Y.; Hu, J.; Li, Y.; Zhang, G.; Zhao, S., Gravity-driven and high flux super-hydrophobic/super-oleophilic poly(arylene ether nitrile) nanofibrous composite membranes for efficient water-in-oil emulsions separation in harsh environments. *Composites Part B: Engineering* **2019,** *177*, 107439.
52. Hlavacek, M., Break-up of oil-in-water emulsions induced by permeation through a microfiltration membrane. *Journal of Membrane Science* **1995,** *102*, 1-7.
53. Sun, D.; Duan, X.; Li, W.; Zhou, D., Demulsification of water-in-oil emulsion by using porous glass membrane. *Journal of Membrane Science* **1998,** *146* (1), 65-72.
54. Hu, B.; Scott, K., Influence of membrane material and corrugation and process conditions on emulsion microfiltration. *Journal of Membrane Science* **2007,** *294* (1), 30-39.
55. Maartens, A.; Jacobs, E. P.; Swart, P., UF of pulp and paper effluent: membrane fouling-prevention and cleaning. *Journal of Membrane Science* **2002,** *209* (1), 81-92.

TOC

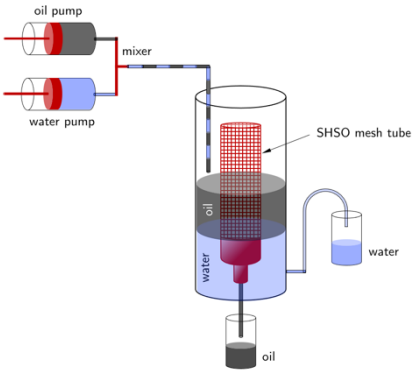
oil pump
mixer
water pump
SHSO mesh tube
oil
water
water
oil

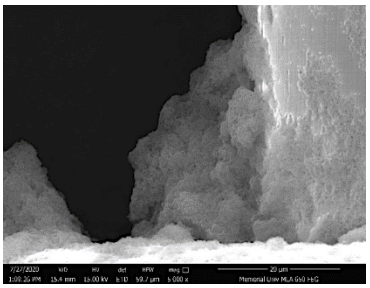

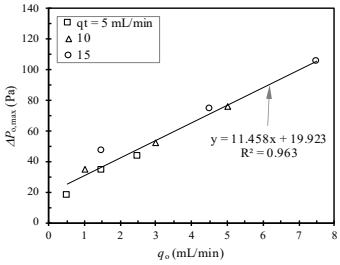
qt = 5 mL/min
10
15
y = 11.458x + 19.923
R² = 0.963
$\Delta P_{o,max}$ (Pa)
q_o (mL/min)
0
20
40
60
80
100
120
140
0
1
2
3
4
5
6
7
8